Evaluation of the Capabilities of a Hybrid Driven Exoskeleton in Passive Mode of Interaction

Dimitar Chakarov[a], Ivanka Veneva[b], Pavel Venev[c] and Mihail Tsveov[d]

Institute of Mechanics, Bulgarian Academy of Sciences, "Acad. G. Bonchev" str., Block 4, Sofia 1113, Bulgaria

Keywords: Exoskeleton Arm, Electric Motors, Pneumatic Cylinders, Interaction Force, Patient, Harmonic Motion, Mechanical Impedance, Experiments, Simulations.

Abstract: A new construction of upper limbs exoskeleton with hybrid drive was studied in this work. The paper presents mechanical structure and actuation of exoskeleton with hybrid drive including pneumatic cylinders and electric motors. In order to evaluate the transparency and safety, the capabilities of the exoskeleton in passive mode of interaction was estimated. A model of the interaction force between the patient and the exoskeleton arm in passive mode was built. The model was based on harmonious movements imposed in one joint of the exoskeleton arm. Experiments and simulations were performed to assess the interaction force between the patient and the exoskeleton because of the mechanical impedance of the device. The force of interaction was obtained from passive forces, such as inertial, frictional and gravitational forces, as well as from the elasticity of the pneumatics. The patient-initiated harmonic motion was studied in two cases- without pressure in the chambers and with pressure for gravity compensation. The results where demonstrated graphically. Conclusions where made about the behavior of the exoskeleton in the passive mode of interaction.

1 INTRODUCTION

Robotic rehabilitation using exoskeletons is an alternative to conventional manual therapy to improve motor function in post-stroke patients (Manna, 2018). The rehabilitation exoskeleton (Jarrasse, 2014) should be able to create a great force for assisting and directing the patient's hand in the early stages of recovery, as well as following the human hand without opposition or being able to react to any movement made by the patient in the full stage of recovery. In the control design of the rehabilitation exoskeleton in general, two "extreme" ideal regimens can be defined, covering the entire spectrum of therapeutic interventions: "robot in charge" and "patient in charge" (Veneman, 2006).

In the "robot in charge" regime, it is important that the robot has enough strength and power to realize the desired movement with a relatively high impedance. In a "patient in charge" it is important that the forces of interaction between the exoskeleton and the patient are low; in other words, the perceived impedance of the robot should be low. The main feature here is transparency.

There are two main approaches to reducing the mechanical impedance of the rehabilitation exoskeletons and to ensure security and transparency in interaction: active and passive. Electric motors, pneumatic, hydraulic and other active drives are used to reducing the impedance and to control the contact force through an active approach. The active approach is based on sensors and algorithms for motor control. There are two methods to control the contact force: direct and indirect. In the direct approach, the controller regulates the force with a control loop and using force feedback of the measurement and desired value of the force (Ansarieshlaghi, 2019). Indirect force control methods are known as impedance or admittance (Hogan, 1985). Impedance controlled systems detect the deviation in position and control the force applied by the device, while admittance controlled systems

---

[a] https://orcid.org/0000-0002-2312-5725
[b] https://orcid.org/0000-0001-5501-7668
[c] https://orcid.org/0000-0001-7809-3540
[d] https://orcid.org/0000-0001-5051-4411

detect the contact force and control the position and velocity or the device.

The passive approach involves passive or inherently safe drives. The pneumatic actuation allows force control according to the active approach. Also, pneumatic actuation has a natural flexibility and allows to achieve inherent safety and transparency in the process of rehabilitation in a passive way (Morales, 2011). Due to the inherent natural compliance of air and its storage in closed chambers, pneumatic actuation can create passive support force.

There are three types of pneumatic drives: pneumatic cylinders, pneumatic artificial muscles (PAM) and rotating pneumatic motors. High natural compliance and non-linearity of air compression of pneumatic drives result in a low dynamic force response, which limits the efficiency of the actuator. To take advantage of pneumatic actuators while reducing their shortcomings, they are combined with electric drives. (Rouzbeh, 2019) integrates a low friction pneumatic cylinder and a rotating electric motor into a compact device. A similar design of hybrid propulsion including a linear electric motor and pneumatic cylinder is presented in (Nakata, 2015). The hybrid pneumatic and electric actuator, compared to high-gear electric drive, produces a lower impedance while maintaining a high driving force value.

A pneumatically driven exoskeleton for training and rehabilitation, aided by interactions in virtual scenes, was developed by the authors. PAM bundles included in an antagonistic circuit are used for propulsion. In order to overcome the shortcomings of pneumatic muscles, the possibilities of using a hybrid drive involving a pair of PAM bundles and a parallel working DC motor are explored (Chakarov, 2019). The structure of the exoskeleton is further developed with hybrid drive, integrating pneumatic cylinders and electric motors.

The subject of the present work is the study of the mechanical structure and the actuation of the hybrid exoskeleton with pneumatic cylinders and electric motors. The aim of this study is to evaluate the transparency and safety by assessing the interaction force between the patient and the exoskeleton in passive mode. Experiments and simulations for estimating the interaction force which is a result of the mechanical impedance of the device are object of the present work.

2 MECHANICAL DESIGN AND ACTUATION OF THE UPPER LIMBS EXOSKELETON

To design a rehabilitation exoskeleton of the upper limbs, which provides transparency and natural safety, it is necessary to build a structure with low values of mechanical impedance. This means that the exoskeleton has extremely light segments attached to the limbs and all heavy components are placed on the back or ground. An exoskeleton of the upper limbs is designed in a similar manner as shown in the diagram of Figure 1 and the photograph of Figure 2. The mechanical structure of the exoskeleton system includes two arms R and L, arranged on a fixed base 0, as each arm includes two identical rotating joints respectively for clavicular motions J1, J2, shoulder motions J3, J4 and elbow motions J5, J6 (Figure 1). The arm has a total of 6 degrees of mobility (h = 6), resembling the natural movement of the human arm from back to elbow. Structure in Figure 1 is chosen in order to design an exoskeleton arm, in which modules with two equal type universal joints are created and so, unlike other solutions, circular guide and three axes joints are avoided. Each arm of the exoskeleton is composed of six movable segments (1, 2, 3, 4, 5 and 6) made mainly of aluminium alloy. The plastic shells with straps are placed on the segments for attachment to a human limb (Figure 2). The generalized masses of the six main segments of the arm are $M_1 = 0.463$ kg, $M_2 = 0.321$ kg, $M_3 = 0.497$ kg, $M_4 = 0.782$ kg, $M_5 = 0.510$ kg and $M_6 = 0.793$ kg.

The arm and forearm lengths of the exoskeleton are set with initial lengths $L_1 = 0.286$ m and $L_2 = 0.370$ m. Their construction includes lightweight ball bearings in aluminium housings and built-in position sensors in their cavity. A high-precision rotary sensor (BOURNS AMS22B) is used to measure the effective displacement. The ranges of movements in the joints
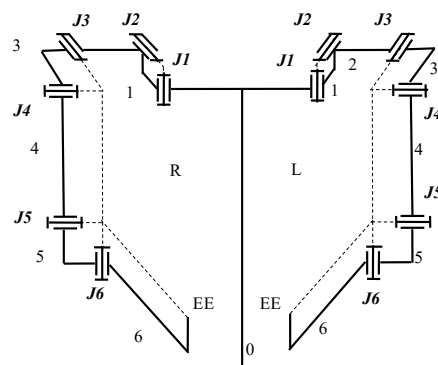

Figure 1: Constructive diagram of a two-handed exoskeleton.

are as follows: $J_1(15°)$, J_2 $(15°)$, $J_3(120°)$, J_4 $(120°)$, J_5 $(150°)$, J_6 $(135°)$. They are consistent with the workspace of the human hand, as shown in (Abane, 2016).

In order to build an actuation that produces a low impedance while maintaining a high value of the driving force, the hybrid approach was chosen, including pneumatic and electric drives operating in parallel.
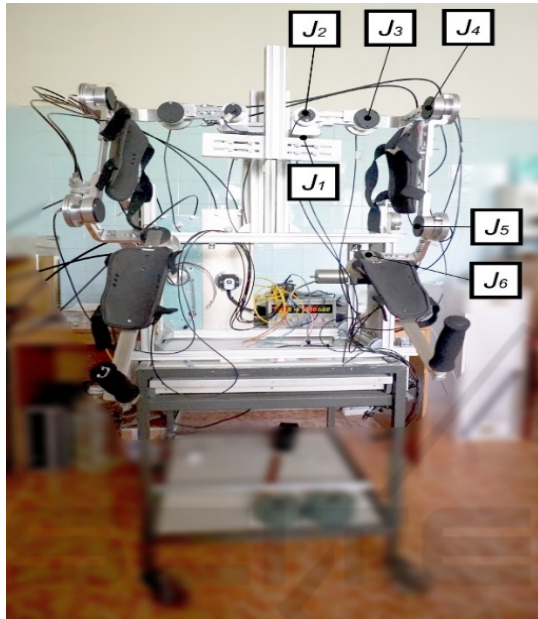

Figure 2: Prototype of a two-handed exoskeleton.

The hybrid actuation of each joint of the exoskeleton is built as a separate unit located in the fixed base. A picture of the drive unit of the joint J_4 in the shoulder is shown in Figure 3. In the base 0 there is a wheel 1 and mounted thereto reel R with a radius equal to 31.5*mm* for winding a cable. Bowden cables T1, T2 were used to connect the reel R and a similar reel located in the joint of the exoskeleton.

The electric drive includes a DC electric motor, on the shaft of which a wheel 3 is mounted (Figure2). The motor is brushless (*MAXON EC 90 flat*), with *Ø90 mm, 260 W, 18V*, nominal torque Q_m=*1010 mNm,* operated with *ESCON Module 50/8 HE* driver.

To transmit movement from wheel 3 of DC motor to wheel 1, a backdrivable transmission is used, including two timing belts B2 and B1 and two wheels 4 and 2 with common shaft. The first gear B2 connects wheels - 3 and 4 and the second gear B1 connects wheels 2 and 1. The first stage of the transmission have gear ratio $n_1 = 3:1$ and the second stage - gear ratio $n_2 = 2:1$. The overall gear ratio is $n = 6:1$.
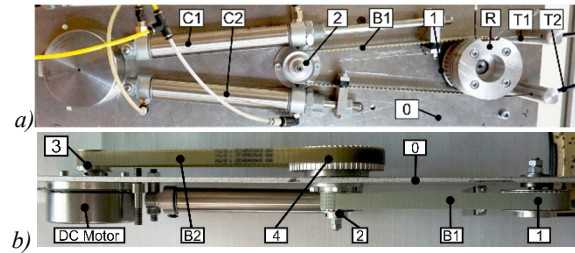

Figure 3: Hybrid actuation unit for the joint J4 of the exoskeleton: (a) front view; b) side view.

The pneumatic drive consists of a pair of pneumatic cylinders, C_1 and C_2 mounted in the base unit 0, as shown in Figure 3. Pneumatic cylinders (*Aignep*) with diameter $D = 0.02$ *m* are used. The cylinders simultaneously drive the opposite sides of the timing belt B1. Two connected chambers of the cylinders are supplied in parallel with compressed air p_a, and the other two chambers with pressure, p_b. The pipes of each pair are connected to two parallel valves (SMC S070-SDG-32), one of which supplies compressed air to the chambers and the other releases the pressure into the atmosphere. Pressure sensors (Honeywell 40PC100G) are mounted on each pipeline.

The torque created by both pneumatic cylinders is

$$Q_p = (p_a(s_1 + s_2) - p_b(s_1 + s_2))r \qquad (1)$$

where p_a and p_b are the supply pressures in both chambers, r is the radius of puley 1 and s_1 and s_2 are the areas on both sides of the piston.

3 MODEL FOR INTERACTION FORCE ASSESSMENT

Experiments have been conducted to assess the force of the interaction in the recovery phase of patients when they are able to initiate complex independent movement in a relatively safe and transparent manner. This is the so-called "patient in charge" stage, where it is important that the forces of interaction between the exoskeleton and the patient are low. If the forces are close to zero it can be said that the exoskeleton is completely "transparent".

To assess the forces of interaction, dynamic experiments were performed with movement in one joint of the exoskeleton, similar to the approach used in (Bembli, 2019). All joints are locked, and joint J4 is controllable, where flexion - extension in the shoulder is performed. The operator moves the exoskeleton arm as shown in Figure 4. The subject of

the present study are the forces in passive mode, when they are defined only by the mechanical impedance of the exoskeleton.

The force of the end effector (EE) applied to the operator's hand, which overcomes the mechanical impedance of the exoskeleton and the actuation, is determined by the inertial, frictional and gravitational forces, as well as the elastic forces according to the equation:

$$F_h = (Q_J + Q_{fr} + Q_g^e + Q_p)/ N \qquad (2)$$

Above N is the value of the radius vector of the EE where force F_h is applied to the patient's hand. In equation (2), the joint torque Q_J is result of the motor and the transmissions inertia as well as the exoskeleton inertia according to equality

$$Q_J = (J_m \frac{n^2}{\eta}\ddot{q} + J_{tr} \frac{n_2^2}{\eta}\ddot{q} + J_e\ \ddot{q}) \qquad (3)$$

Here, J_m represents the inertia of the motor and wheel 3, J_{tr} represents the inertia of the transmission wheels 2 and 4, J_e represents the inertia of the exoskeleton and wheel 1. Above n is the overall transmission gear ratio, n_2 is the gear ratio of second stage, η is transmission efficiency, for the case, when the motor is driven by human (Giberti, 2010).

In equation (2) Q_{fr} represents the friction torque which is mainly the result of the friction forces generated in pneumatic actuators and Bowden cables. The friction force for each side of the parallel drive can be represented by the following equation

$$F_{fr} = F_c\ sign(\dot{x}) + B\dot{x} \qquad (4)$$

where: F_c represents the Columbus friction force, B is viscous damping coefficient and $\dot{x}$ is cable velocity. These coefficients represent a general estimate of the various energy effects in pneumatic cylinders, Bowden cables, DC motors, etc., for which empirical rather than analytical estimates are known (Andrighetto, 2006), (Schiele, 2006). The EE friction torque as a result of the friction forces of the parallel drive is

$$Q_{fr} = 2F_{fr}r \qquad (5)$$
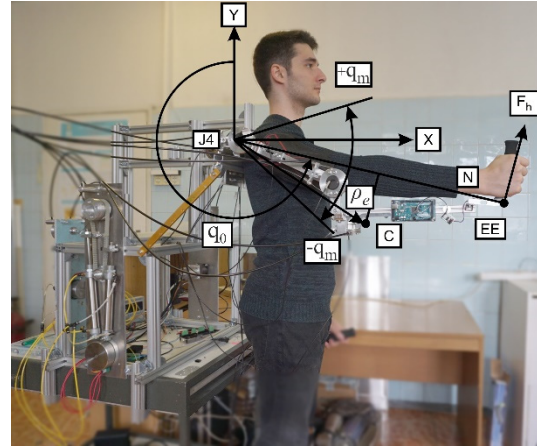
where r is radius of pulley 1.

Figure 4: Harmonic motion imposed by the operator on the exoskeleton joint J4.

In equation (2), Q_g^e is the torque resulting from the exoskeleton gravity according to the equation

$$Q_g^e = M_e g(\rho_{e1} sinq + \rho_{e2} cosq) \qquad (6)$$

where: M_e represents the mass of exoskeleton moving parts 4, 5, 6; $\rho_e = [\rho_{e1}; \rho_{e2}]^T$ represents the radius vector of the mass center C in a local frame and g is the gravity acceleration coefficient.

In equation (2) with Q_p is denoted the torque of the pneumatic drive as a result of the elastic forces due to air compressibility of the chambers of the both pneumatic cylinders (C1 and C2), (Figure 5).
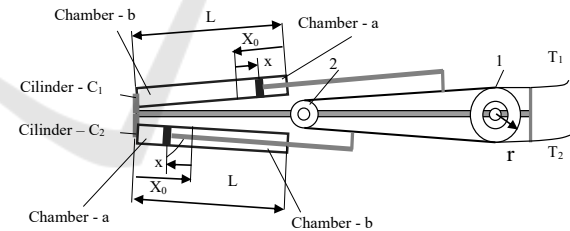

Figure 5: Scheme of the pneumatic drive of the exoskeleton joints.

Assuming that air is an ideal gas undergoing an isothermal process, the change in pressure inside each chamber (a,b) of the two connected cylinders can be expressed according to (Shen, 2007) as the ratio of the mass flow rate to the volume of the chamber as follows

$$p_{(a,)} = \frac{m_{(a)}RT}{(X_0 - x)(s_1 + s_2)} \qquad (7)$$

$$p_{(b)} = \frac{m_{(b)}RT}{(L - X_0 + x)(s_1 + s_2)} \qquad (8)$$

where: $m_{(a)}$, $m_{(b)}$ are the mass flow rate entering the chamber (a, b); R is the universal gas constant, T is the gas temperature at the orifice, x is the piston displacement measured from starting position X_0 for actuator C_1 and C_2 according to the scheme of Figure 4. In equations (7), (8) the volumes of the connected chambers are taken into account where s_1 and s_2 are the areas on both sides of the piston.

In the conducted experiment it was accepted, that one chamber of the pneumatic cylinders is supplied with a pressure p_{a0} and the other p_{b0}, after which the supply and discharge valves of the pneumatic cylinders are closed. It is assumed that this is done in the starting position of the cylinders X_0, where $x = 0$. In this position the pressure inside each chamber (a,b) of the cylinders can be expressed as follows

$$p_{(a)}^{0} = \frac{m_{(a)}RT}{(X_0)(s_1 + s_2)} \qquad (9)$$

$$p_{(b)}^{0} = \frac{m_{(b)}RT}{(L - X_0)(s_1 + s_2)} \qquad (10)$$

After excluding the general parameters from (9), (10) to (7), (8), the equations for changing the pressures in the chambers of the cylinders when changing their strokes are obtained as follows

$$p_{(a)} = \frac{p_{(a)}^{0} X_0}{(X_0 - x)} \qquad (11)$$

$$p_{(b)} = \frac{p_{b}^{0}(L - X_0)}{(L - X_0 + x)} \qquad (12)$$

The elastic torque created by both pneumatic cylinders is determined by (1), where the pressures in the connected cylinder chambers are represented by (11), (12). After substituting in (1) it is obtained the equality of elastic torque as a result of the pistons deviation x from the starting position X_0

$$Q_p = [\frac{p_a^0 X_0}{X_0 - x} - \frac{p_b^0(L - X_0)}{L - X_0 + x}](s_1 + s_2)r \quad (13)$$

When the starting position X_0 of the cylinders corresponds to the initial position of the arm q_0, (Figure: 3) the displacements x of the pistons from the starting position depend on the deviations q of the joint angle from the initial position q_0 as follows

$$X = qr \qquad (14)$$

4 EXPERIMENTS AND SIMULATIONS FOR EVALUATION OF INTERACTION FORCE IN PASSIVE MODE

In this mode, the authors suggest that the patient has the motor capacity to move his hand independently and intensively. In passive mode, the electric and pneumatic drives do not generate active forces. The operator performs harmonic movements from the original position with equal amplitude and constant oscillation frequency. The angle q in the joint J4 determines the position of the arm, assuming that $q = 0$ when the arm coincides with the Y axis (Figure 4). To measure the interaction force, a load cell is located on the end effector, where the force is applied to the operator's hand.

4.1 Passive Mode of Interaction without Pressure in the Chambers

A. Experiments. In this experiment, a passive mode is realized, as the valves of the pneumatic actuator are open to the atmosphere ($p_a = 0$ and $p_b = 0$) and no voltage is applied to the electric actuator. The human operator has performed harmonic movements from the initial position $q_0 = 260^0$ at an amplitude of about $q_m = 20^0$ with an oscillation frequency of about $\omega = 2.1$ rad/s. The forces applied by the hand of operator to overcome the mechanical impedance of the exoskeleton changes as shown in Figure 6 a). As can be seen from the experiment, the interaction force has an average value of -8.2 N determined mainly by the weight of the exoskeleton. Dynamic deviations around it are about ±2 N.

B. Simulations. To assess the parameters of the actuators and to evaluate the correctness of the constructed mathematical model, dynamic simulations of the movements in joint J4 are conducted. To model the harmonic motions from the initial position q_0 with amplitude q_m and oscillation frequency ω, the following law of motion is used

$$q = q_m \sin(\omega t) + q_0 \qquad (15)$$

as well as the laws of velocity and acceleration obtained after differentiation of (15) as presented in (Chakarov, 2020).
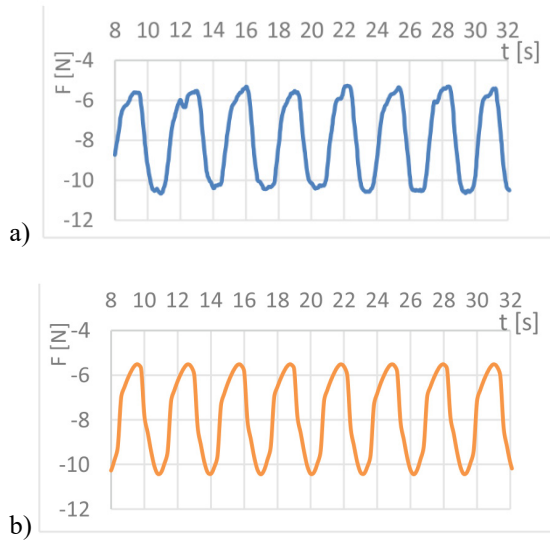
a)

b)

Figure 6: Interaction force in passive mode without pressure in the chambers: a) experiment; b) simulation.

The simulations were conducted with the same values of the kinematic parameters used in the previous experiment: starting angle $q_0 = 260°$, amplitude $q_m = 20°$ and frequency of $\omega = 2.1$ rad/s.

The forces applied by the hand of human operator to overcome the mechanical impedance of the exoskeleton are calculated according to equation (2). The graph in Figure 6 b) shows the change in the interaction force (2) as result of the inertia torque (3), the friction torque (5) as well as the exoskeleton gravity (6). The values of the mechanical parameters using for calculations with equations (3) – (6) are shown in Table 1.

4.2 Passive Mode of Interaction with Gravity Compensation

A. Experiments. In this experiment, the exoskeleton arm is gravitationally compensated in the initial position q_0. For this purpose, one chamber of the pneumatic cylinders is supplied with a pressure equal to $p_a = 250$ kPa and the other - $p_b = 0$, after which the supply and discharge valves of the pneumatic cylinders are closed. In this case, the passive forces applied by the operator hand are result not only of the sources mentioned in the previous experiment but also of the forces Q_p resulting from the compressibility of the air in the cylinder chambers. The operator has performed harmonic movements, from the initial position $q^0 = 260^0$, with amplitude of about $q_m = 23^0$ and frequency of about $\omega = 2.7$ rad/s. The change in interaction force is shown in Figure 7

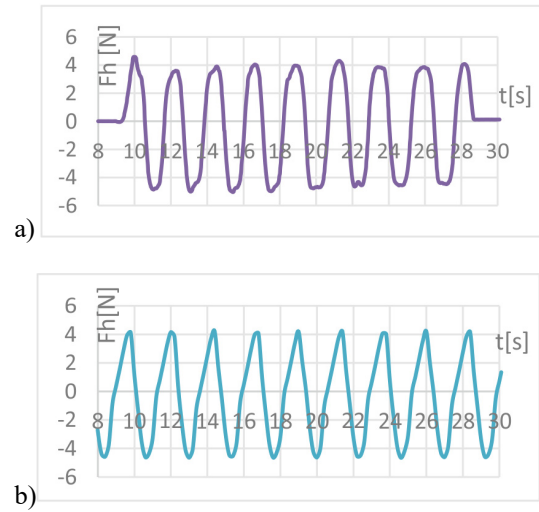a). The experiment shows a force change in both directions about ±4.5 N.

a)

b)

Figure 7: Interaction force in passive mode with gravity compensation: a) experiment; b) simulation.

Table 1: Electric and pneumatic drives parameters.

Parameter name		Value	
Motor efficiency	η_m	90	%
Motor inertia	J_m	508.10^{-6}	kgm^2
First stage reduction	n_1	3 : 1	
Second stage reduction	n_2	2 : 1	
Transmission efficiency	η_{tr}	97	%
Transmission inertia	J_{tr}	$173 \cdot 10^{-6}$	kgm^2
Piston area side 1	s_1	$314 \cdot 10^{-6}$	m^2
Piston area side 2	s_2	$264 \cdot 10^{-6}$	m^2
Pneumatic cylinder diameter	D	0.020	m
Pneumatic cylinder stroke	L	0.125	m
Piston starting position	X_0	0.050	m
Actuation viscous friction	B	665	Ns/m
Actuation Coulomb friction	F_c	8.61	N
Exoskeleton mass	M_e	2.085	kg
Exoskeleton inertia	J_e	0.198	kgm^2
Radius of EE	N	0.660	m
Radius of pulley 1	r	0.0315	m
Coordinate 1 of mass center	ρ_{e1}	0.256	m
Coordinate 2 of mass center	ρ_{e2}	0.031	m

B. Simulations. In the conducted simulation, the interaction force includes all components according to equation (2). The torque of the pneumatic drive (13) is calculated in the initial position q_0 with pressures of the two chambers, respectively $p_a = 250$

kPa and $p_b = 0$. The same harmonious movement as in the previous experience is simulated with the kinematic parameters: starting position $q_0 = 260°$, amplitude $q_m = 23°$ and frequency of $\omega = 2{,}7$ rad/s. Figure 7 b) shows the force of interaction which is the result of the sum of dynamic forces, gravity forces and elastic forces in the chambers of the pneumatic cylinders. The elastic force acts as an elastic balancer of the gravity load. The interaction force is 0 at the initial position and fluctuates ± 4.5 N around this value, as in the previous experiment.

5 CONCLUSIONS

The paper reveals the mechanical design of an exoskeleton of the upper limbs, which uses the scheme of hybrid drive with electric and pneumatic actuation, thus producing a lower impedance due to pneumatics, while maintaining high driving force and rapid force response due to electric actuation. Further reduction of the mechanical impedance is achieved by placing the components of the hybrid drive in the fixed base.

Several experiments with the available mechanical prototype of the exoskeleton were performed in the work to test the hypothesis that the proposed hybrid drive is able to provide the two modes of interaction: a) "robot in charge" mode, when the exoskeleton applies forces with high impedance and b) "patient in charge" mode when the forces of interaction with the operator are low due to the reduced impedance of the robot.

In the experiments, the force between the operator and the exoskeleton was evaluated. The force of interaction was obtained from passive forces, which are the result of inertia, friction and gravity, as well as the elasticity of pneumatics. In "patient in charge" way the patient-initiated harmonic motion was studied in two cases - without pressure in the chambers and with pressure for gravity compensation.

In the first case, the force of interaction determined mainly by the exoskeleton gravity indicates that the exoskeleton arm is relatively heavy ($F_h = -8.2$ N). As a result of added inertia and friction forces from harmonic movements, this force oscillates from -5.8 to -10.2 N. When gravity is compensated passively by pressure in the chambers of pneumatic cylinders, the force of interaction is determined by the elastic forces of compressed air, as well as by the inertia forces and friction. For the selected harmonic deviations, the force of interaction reaches relatively high values ($Fh = \pm 4.5$ N).

The work also includes several computer experiments to assess the parameters of the actuators and the correctness of the constructed mathematical model. Computer experiments show a similar change in the interaction force as in the real experiment. It can be noted that the parameters introduced in the model such as exoskeleton mass and coefficients of Coulomb and viscous friction in the actuators (Table 1) have quite high values.

The conducted experiments show that the resulting forces of interaction in passive mode are essential in terms of transparency, but are not a threat of security. In active mode of operation, the forces of interaction can be reduced by active compensations, but the created low values of the forces in passive mode are a guarantee of general security.

The design and control of this exoskeleton are under development. Future work will be done by incorporating the controller and assessing the transparency and safety of the interaction between the patient and the exoskeleton in active mode.

ACKNOWLEDGEMENTS

REFERENCES

Manna S. K., Dubey V. N., 2018. Comparative study of actuation systems for portable upper limb exoskeletons, *Medical Engineering and Physics,* 60, 1–13.

Jarrasse, N., T. Proietti, et al., 2014. Robotic Exoskeletons: A Perspective for the Rehabilitation of Arm Coordination in Stroke Patients, *Frontiers in Human Neuroscience,* Vol.8, Art.947, 1-13.

Veneman, J.F., R. Ekkelenkamp, et al., 2006. A series elastic- and bowden-cable-based actuation for use as torque actuator in exoskeleton-type robots, *The Int. Journ. of Rob. Research,* vol. 25(3), 261-281.

Hogan N., 1985. Impedance Control: An Approach to Manipulation, *ASME J. Dynamic Systems Meas. & Control,* 107: 1-24.

Ansarieshlaghi, F. and P. Eberhard, 2019. Hybrid Force/Position Control of a Very Flexible Parallel Robot Manipulator in Contact with an Environment. *In Proc. of the 16th International Conference on Informatics in Control, Automation and Robotics (ICINCO 2019),* Vol.2, 59-67.

Morales R., et al., 2011. Pneumatic robotic systems for upper limb rehabilitation, *Med. Biol. Eng. Comput*. 49, 1145–1156.

Rouzbeh B., et al.,2019. Design, Implementation and Control of an Improved Hybrid Pneumatic-Electric Actuator for Robot Arms, *IEEE Access*, Vol. 7, 14699 – 14713.

Nakata Y., T. Noda, J. Morimoto, and H. Ishiguro, 2015. Development of a pneumatic-electromagnetic hybrid linear actuator with an integrated structure, *Proc. IEEE/RSJ Int. Conf. Intell. Robots Syst.,* Sep./Oct. 2015, 6238–6243.

Chakarov D., Veneva I., Tsveov M., Mitrouchev P., Venev P., 2019. Design of a Two Arms Exoskeleton as Haptic Device for Virtual Reality Applications, *Lecture Notes in Mech. Eng., Springer Nature*, Chapter 25, 252-262.

Abane, A., Guiatni, et al., 2016. Mechatronics Design, Modeling and Preliminary Control of a 5 DOF Upper Limb Active Exoskeleton, *Proc. of the 13th Int. Conf. on Informatics in Control, Automation and Robotics (ICINCO 2016), Vol. 2*, 398-405

Bembli, S., Haddad, N. and Belghith, S., 2019. A Terminal Sliding Mode Control using EMG Signal: Application to an Exoskeleton- Upper Limb System. *Proc. of the 16 th Int. Conf. on Informatics in Control, Automation and Robotics (ICINCO 2019),* Vol.2, 559-565.

Giberti H, Cinquemani S, and Legnani G., 2010. Effects of transmission mechanical characteristics on the choice of a motor-reducer. *Mechatronics;* 20(5), 604–610.

Andrighetto P., Valdiero A., Carlotto L., 2006. Study of the friction behavior in industrial pneumatic actuators. *ABCM Symposium Series in Mechatronics*, Vol. 2, 369-376.

Schiele A., Letier P. et al., 2006. Bowden cable actuator for force-feedback exoskeletons*. IEEE Int. Conf. on Intelligent Robots and Systems*: 3599-3604.

Shen X. and M. Goldfarb, 2007. Simultaneous force and stiffness control of a pneumatic actuator, *Journal of Dynamic Systems Measurement and Control,* vol. 129, no. 4, 425–434.

Chakarov D, Iv. Veneva, M. Tsveov, P. Venev, 2020. Study of a Hybrid Actuated Exoskeleton for Upper Limb Rehabilitation, *Proc. of the 17th International Conference on Informatics in Control, Automation and Robotics, ICINCO 2020*, Vol. 1, 498-505.